Int. J. Heat Mass Transfer. Vol. 27, No. 12, pp. 2277–2287, 1984
Printed in Great Britain

0017–9310/84 $3.00 + 0.00

Thermal convection in a horizontal, eccentric annulus containing a saturated porous medium—an extended perturbation expansion

HAIM H. BAU

Department of Mechanical Engineering and Applied Mechanics, University of Pennsylvania, Philadelphia, PA 19104, U.S.A.

(*Received* 17 *January* 1984 *and in revised form* 30 *March* 1984)

Abstract—Thermal convection in a saturated porous medium confined between two horizontal, isothermal, eccentric cylinders is studied through the use of a regular perturbation expansion in terms of the Darcy–Rayleigh number (R). Terms up to $O(R^{30})$ are computed. In particular, the Nusselt number (Nu) is expressed as a power series of R for various eccentricities. The above power series has, however, a limited radius of convergence. Various non-linear transformations are employed in order to extend the range of utility of the series. The results are used to demonstrate that the heat transfer in the annulus can be optimized by a proper choice of eccentricity. These results have a bearing on the design of thermal insulators.

1. INTRODUCTION

NATURAL convection in porous media is germane to many technologies involving thermal insulators such as: steam lines, gas lines in gas-cooled nuclear reactors, cryogenics, and storage of thermal energy, to name just a few. The thermal insulator typically consists of a fibrous material, which is permeable to fluid motion. Consequently, natural convection may develop in the insulating material and contribute significantly to the heat transfer process, as has been demonstrated by Caltagirone [1], Burns and Tien [2], Brailovskaya *et al.* [3], and others. Currently, concentric insulations are widely used. Clearly, for a horizontal pipe, an eccentric insulation may be more efficient and more economical than a concentric one since the heat transfer process in the insulation consists of natural convection and conduction. An increase in the eccentricity so that the center of the inner, hotter cylinder is above the center of the outer one reduces the effective Darcy–Rayleigh number and therefore the impact of the convective heat transfer. On the other hand, the resulting reduction in the local thickness of the insulation may increase the conductive heat losses. Hence, one may expect that an optimal value of eccentricity exists for which the heat losses are minimized.

The effects of eccentricity on the heat transport in an annulus containing viscous fluid (a non-porous medium) has been studied experimentally [4] and numerically [5–7]. The analogous problem of a permeable, annular medium has attracted, however, much less attention.

In a previous study [8], a regular perturbation expansion in terms of the Darcy–Rayleigh number was used to study the flow and temperature fields inside the eccentric annulus. In the above work [8], the governing equations were solved analytically. Only the three first terms could be calculated in the expansion, up to $O(R^3)$, before a state of exhaustion had been reached. Consequently, the results of ref. [8] are valid only for small R numbers. In this paper, Van Dyke's recommendations [9, 10] are followed and the cumbersome task of calculating higher order terms is delegated to the computer. This enables the Nusselt number to be expressed as a power series of R up to $O(R^{30})$. The above series, however, has a limited radii of convergence. The radii of convergence of the series is estimated using the Cauchy root test (Section 4). Then, the range of utility of the series is extended through various nonlinear transformations such as: series reversal (Section 5), Padé approximants (Section 6), and Shank's transformation (Section 7). The results of this study are compared with calculations obtained using other numerical techniques (Section 8), and, finally, it is demonstrated that the heat transfer in the annulus can indeed be optimized by a proper choice of the eccentricity.

2. THE MATHEMATICAL MODEL

Consider an eccentric annulus, of inner and outer radii $\hat{r}_1$ and $\hat{r}_2$, containing a saturated porous medium (Fig. 1). The cylinder's surfaces are impermeable and are maintained at constant uniform temperatures, $\hat{T}_1$ and $\hat{T}_2$, respectively. As a result of the above temperature difference, fluid motion is induced in the medium.

The problem is formulated using bicylindrical coordinates [11]. The conversion into bicylindrical coordinates is achieved through the transformation [11]

$$x+\mathrm{i}\,y = a\coth\frac{\alpha-\mathrm{i}\,\beta}{2} \tag{1}$$

NOMENCLATURE

a	scale factor in bicylindrical coordinates, $\sinh \alpha_1$
e	eccentricity
g	gravity vector
G, H	functions, equation (5)
N_s	a coefficient in the expansion for the Nusselt number
Nu	Nusselt number
Q	heat flow
q	heat flux
R	Rayleigh–Darcy number, $\beta^* g \lambda \hat{r}_1 (\hat{T}_1 - \hat{T}_2)/\alpha_{eq} \nu$
R_c	radius of convergence of the perturbation series
r	cylinder radius
T	temperature
x, y	Cartesian coordinates.

Greek symbols

α, β	bicylindrical coordinates
α_{eq}	equivalent thermal diffusivity of the saturated porous medium
β^*	thermal expansion coefficient
θ	inclination angle
λ	permeability
ν	kinematic viscosity
ρ	density
ψ	stream function.

Subscripts

1	inner cylinder surface
2	outer cylinder surface.

Superscript

$\hat{}$	dimensional variables.

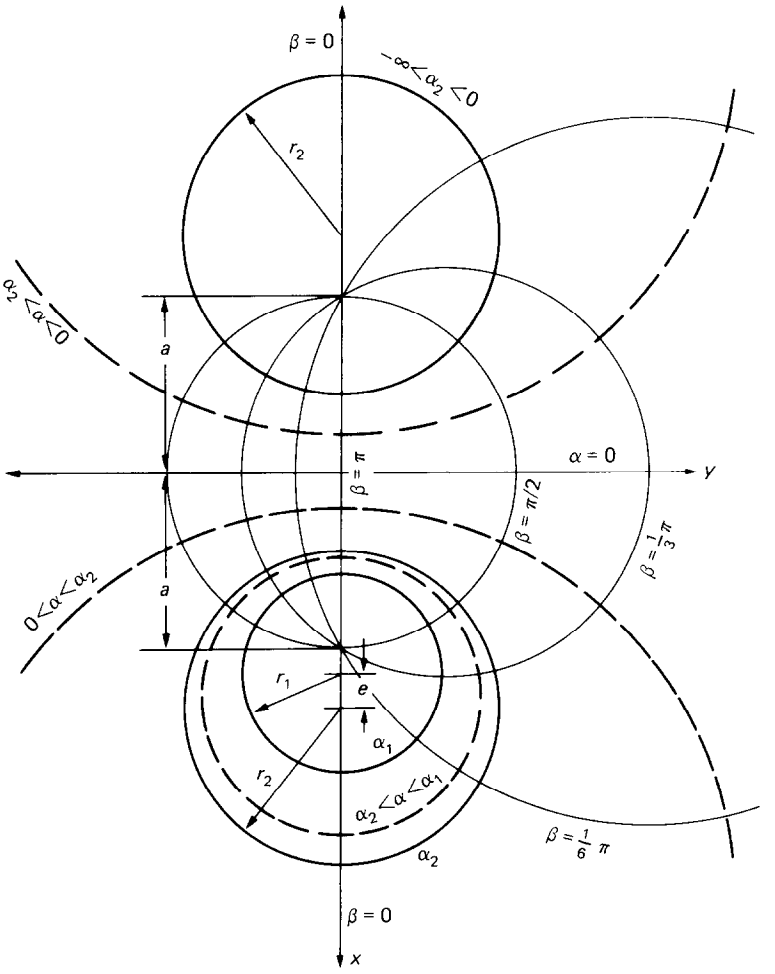

FIG. 1. The coordinate system.

where constant α coordinates are the circles

$$(x-a\coth\alpha)^2+y^2=\frac{a^2}{\sinh^2\alpha}. \tag{2}$$

The bicylindrical coordinates are natural for this problem since the physical boundaries (the cylinder's surfaces, $\hat{r}_1$ and $\hat{r}_2$) are identified with constant value coordinates $\alpha_1>0$ and $0<\alpha_2<\alpha_1$, respectively (Fig. 1). The corresponding radii ratio is $\hat{r}_2/\hat{r}_1=\sinh\alpha_1/\sinh\alpha_2$, the eccentricity $\hat{e}/\hat{r}_1=\sinh(\alpha_1-\alpha_2)/\sinh\alpha_2$, and $\hat{a}=\hat{r}_1\sinh\alpha_1$. The superscript carot ($\hat{}$) denotes dimensional quantities which later will be made non-dimensional. One can note that for any given radii ratio and eccentricity, two corresponding values of α_1 and α_2 can be found. One drawback of this coordinate system is that it does not provide for concentric cylinders. However, one may decrease the eccentricity as much as one desires. Thus, from the practical point of view, this limitation is not a serious one.

The dimensionless Darcy–Oberbeck–Boussinesq's equations formulated in terms of the stream function (ψ) and the temperature (T) have the following form

$$\begin{aligned}\frac{\partial^2\psi}{\partial\alpha^2}+\frac{\partial^2\psi}{\partial\beta^2}&=\pm aR\left\{G(\alpha,\beta)\frac{\partial T}{\partial\alpha}+H(\alpha,\beta)\frac{\partial T}{\partial\beta}\right\}\\ \frac{\partial^2T}{\partial\alpha^2}+\frac{\partial^2T}{\partial\beta^2}&=\frac{\partial\psi}{\partial\alpha}\frac{\partial T}{\partial\beta}-\frac{\partial\psi}{\partial\beta}\frac{\partial T}{\partial\alpha}\end{aligned} \tag{3}$$

with the following boundary conditions

$$\begin{aligned}&\psi=0;\quad T=1\quad\text{at }\alpha=\alpha_1\\ &\psi=0;\quad T=0\quad\text{at }\alpha=\alpha_2\\ &\psi,T(\alpha,\beta+2\pi)=\psi,T(\alpha,\beta).\end{aligned} \tag{4}$$

The (+) and (−) signs in equations (3) refer, respectively, to the case in which the center of the inner cylinder is above the center of the outer cylinder ($e>0$) and to the case in which the center of the inner cylinder is below the center of the outer cylinder ($e<0$).

The functions G and H are

$$\begin{aligned}H(\alpha,\beta)&=\frac{1-\cosh\alpha\cos\beta}{(\cosh\alpha-\cos\beta)^2}\\ G(\alpha,\beta)&=\frac{\sinh\alpha\sin\beta}{(\cosh\alpha-\cos\beta)^2}.\end{aligned} \tag{5}$$

The equations are written in a non-dimensional form, in which one can scale the length with $\hat{r}_1$, the velocity with $\alpha_{eq}/\hat{r}_1$ and the temperature with $(\hat{T}_1-\hat{T}_2)$. $R=\beta^*g\lambda\hat{r}_1(\hat{T}_1-\hat{T}_2)/\nu\alpha_{eq}$ is the Darcy–Rayleigh number. α_{eq} is the equivalent thermal diffusivity, ν is the fluid kinematic viscosity, β^* is the thermal expansion coefficient, and λ is the medium permeability.

The wall heat flux is

$$q=\left(\frac{\cosh\alpha-\cos\beta}{a}\frac{\partial T}{\partial\alpha}\right)\quad\text{at}\quad\alpha=\alpha_1\quad\text{or}\quad\alpha=\alpha_2. \tag{6}$$

The total heat flow Q is

$$Q=\int_{-\pi}^{\pi}\left(\frac{\partial T}{\partial\alpha}\right)d\beta\quad\text{at}\quad\alpha=\alpha_1\quad\text{or}\quad\alpha=\alpha_2, \tag{7}$$

and the Nusselt number is

$$Nu=\frac{Q_{\text{total}}}{Q_{\text{conduction}}}=\frac{(\alpha_1-\alpha_2)}{2\pi}Q.$$

3. THE SOLUTION PROCEDURE

One can proceed to solve equations (3) and (4) by expanding the dependent variables into a power series in terms of the Darcy–Rayleigh number (R)

$$T=\sum_{s=0}^{S}R^sT_s;\quad\psi=\sum_{s=0}^{S}R^s\psi_s;\quad\text{and}\quad Nu=\sum_{s=0}^{S}R^sN_s. \tag{8}$$

Next, equation (8) is introduced into equation (3), terms of like power in s are compared and at each level of s a set of linear partial differential equations is obtained. Before proceeding to solve the above equations, it is convenient to expand H and G, equation (5), into their corresponding Fourier series [8, Appendix A]. The equations at level s are

$$\begin{aligned}\frac{\partial^2\psi_s}{\partial\alpha^2}+\frac{\partial^2\psi_s}{\partial\beta^2}&=2a\sum_{k=1}^{\infty}k\,e^{-k\alpha}\\ &\quad\times\left[\frac{\partial T_{s-1}}{\partial\alpha}\sin k\beta-\frac{\partial T_{s-1}}{\partial\beta}\cos k\beta\right]\\ \frac{\partial^2T_s}{\partial\alpha^2}+\frac{\partial^2T_s}{\partial\beta^2}&=\sum_{j=1}^{S}\left[\frac{\partial\psi_j}{\partial\alpha}\frac{\partial T_{s-j}}{\partial\beta}-\frac{\partial\psi_j}{\partial\beta}\frac{\partial T_{s-j}}{\partial\alpha}\right]\end{aligned} \tag{9}$$

with boundary conditions

$$\begin{aligned}\psi_0=0,\quad T_0=1\quad\text{at }\alpha=\alpha_1\\ \psi_0=0,\quad T_0=0\quad\text{at }\alpha=\alpha_2\end{aligned} \tag{10}$$

and

$$\psi_s=T_s=0\quad\text{at }\alpha=\alpha_1,\alpha_2\quad\text{for }s>0.$$

The contribution to the Nusselt number is

$$N_s=\frac{\alpha_2-\alpha_1}{2\pi}\int_{-\pi}^{\pi}\left(\frac{\partial T_s}{\partial\alpha}\right)d\beta\quad\text{at }\alpha=\alpha_1\text{ or }\alpha=\alpha_2. \tag{11}$$

Calculations are only carried out for positive eccentricities ($e>0$), since the same results can be easily modified to include negative eccentricities ($e<0$). Also, note that the case of positive eccentricity ($e>0$) and negative Rayleigh number ($R<0$), that is when the inner cylinder is colder than the outer one, is identical to the case of negative eccentricity ($e<0$) and $R>0$ (i.e. the inner cylinder is hotter than the outer one).

In order to solve the Poisson equations, equations (9) and (10), a Galerkin method is used, which applies a

truncated spectral presentation of the form

$$\psi_s(\alpha,\beta)=\sum_{m=1}^{M}\sum_{n=1}^{N}A_{s,m,n}\sin(m\beta)\sin\left(n\pi\frac{\alpha-\alpha_2}{\alpha_1-\alpha_2}\right)$$
$$T_s(\alpha,\beta)=\sum_{m=0}^{M}\sum_{n=1}^{N}B_{s,m,n}\cos(m\beta)\sin\left(n\pi\frac{\alpha-\alpha_2}{\alpha_1-\alpha_2}\right) \quad (12)$$

for $s>0$; and

$$T_0(\alpha,\beta)=\frac{\alpha-\alpha_2}{\alpha_1-\alpha_2},\quad \psi_0=0 \quad \text{for} \quad s=0.$$

Note that the trial functions in the above expressions satisfy the boundary conditions exactly. The matrices of the coefficients $A_{s,m,n}$ and $B_{s,m,n}$ are found by requiring equations (12) to solve equations (9) in the sense of weighted residuals.

Consequently, recursive algebraic relations are obtained for the coefficients $A_{s,m,n}$ and $B_{s,m,n}$. The detailed expressions are listed in Appendix A. Once the coefficients $B_{s,m,n}$ are known, the coefficients N_s in the power series for the Nusselt number (Nu) can be determined from

$$N_0=1$$
$$N_s=\pi\sum_{n=1}^{N}nB_{s,0,n}\quad (s>0). \quad (13)$$

Some of the computations were carried out on a mainframe (Univac 1100) using double precision Fortran (18 digits precision) and some on a personal computer (PC; HP 9816) using uncompiled Basic (15 digits precision). The time required to calculate 30 terms, with $(M,N)=(18,18)$ in the Galerkin expansion, equation (12), is about 1.5 h on the mainframe and about 79.2 h on the PC. The computational time to obtain the sth term is approximately $0.48+0.17(s-2)$ h on the PC. The results obtained from the mainframe and the PC were identical within at least ten significant digits. Consequently, one can conclude that machine truncation does not adversely affect accuracy. Another issue of concern which is discussed briefly in Appendix B is the sufficiency of the number of terms (M,N) in the spectral representation, equations (12).

In this paper the computation of the rate of heat transfer is focused on. The description of the flow and temperature fields will not be given here, but those results are qualitatively similar to those presented in refs. [8, 12].

The numerical results obtained for N_s are listed in Table 1, for a radii ratio $r_2/r_1=2$ and positive eccentricities, $\hat{e}/(\hat{r}_2-\hat{r}_1)=0.001$, 0.2, 0.4, 0.6 and 0.8. The same coefficients can be applied for negative

Table 1. The coefficients in the series expansion $Nu=\sum_{s=0}^{S}N_sR^s$ for $\hat{r}_2/\hat{r}_1=2$ and various eccentricities $e=0.001$, 0.2, 0.4, 0.6 and 0.8. The radii of convergence (R_c) are listed at the bottom of the table

e	0.001 (20, 20)	0.2 (18, 18)	0.4 (18, 18)	0.6 (20, 20)	0.8 (18, 18)
0	+1.0000E+00	+1.0000E+00	+1.0000E+00	+1.0000E+00	+1.0000E+00
1	+0.0000E+00	+0.0000E+00	+0.0000E+00	+0.0000E+00	+0.0000E+00
2	+1.7276E−04	+1.7403E−04	+1.7586E−04	+1.7123E−04	+1.4484E−04
3	−4.8173E−09	−9.8355E−07	−2.0499E−06	−3.0797E−06	−3.5142E−06
4	−1.6750E−08	−1.3212E−08	−1.1618E−09	+2.0629E−08	+4.3831E−08
5	+1.7167E−12	+3.6015E−10	+7.9856E−10	+1.2751E−09	+1.5201E−09
6	+7.5594E−13	−4.4604E−12	−2.7441E−11	−8.1654E−11	−1.5489E−10
7	−2.5360E−16	+1.7772E−14	+6.3847E−13	+3.0206E−12	+7.5214E−12
8	+2.9256E−16	+4.7540E−16	−9.5031E−15	−6.8229E−14	−2.1268E−13
9	+1.7343E−20	−7.6266E−18	−9.0491E−17	−4.3526E−16	−1.2817E−15
10	−1.4381E−19	+1.3186E−19	+1.6166E−17	+1.4735E−16	+6.0431E−16
11	+2.6933E−23	−1.4651E−20	−8.6776E−19	−9.1163E−18	−4.2864E−17
12	+2.0776E−23	+8.3642E−22	+3.0560E−20	+3.3452E−19	+1.7302E−18
13	−1.4948E−26	−2.6930E−23	−5.9691E−22	−4.6342E−21	−1.9042E−20
14	+4.7960E−27	+4.3197E−25	−9.4010E−24	−3.6747E−22	−3.3211E−21
15	−4.1246E−30	+6.6112E−27	+1.4579E−24	+3.4955E−23	+3.1788E−22
16	+1.9762E−30	−7.4089E−28	−7.2439E−26	−1.6342E−24	−1.5714E−23
17	+1.3363E−33	+2.8521E−29	+2.0795E−27	+3.8317E−26	+3.2225E−25
18	−1.2030E−33	−6.2669E−31	−1.3037E−29	+8.6175E−28	+2.0844E−26
19	+1.9161E−36	+2.1859E−33	−2.3708E−30	−1.4251E−28	−2.6357E−27
20	−8.8014E−37	+4.8416E−34	+1.5830E−31	+8.0057E−30	+1.4874E−28
21	−1.7078E−40	−2.4200E−35	−5.6717E−33	−2.4428E−31	−3.9663E−30
22	+3.7344E−40	+6.6005E−37	+9.2280E−35	−6.0244E−34	−1.3359E−31
23	−4.9603E−43	−8.0407E−39	+3.1839E−36	+5.8152E−34	+2.2878E−32
24	+1.2535E−43	−2.2840E−40	−3.2621E−37	−3.9282E−35	−1.4354E−33
25	+6.4995E−47	+1.7495E−41	+1.4288E−38	+1.4538E−36	+4.5516E−35
26	−7.9607E−47	−5.9019E−43	−3.4243E−40	−1.4084E−38	+7.5186E−37
27	+5.6016E−50	+1.1383E−44	−1.6720E−42	−2.2743E−39	−2.0208E−37
28	+1.0936E−50	+3.6013E−49	+6.2335E−43	+1.9183E−40	+1.4070E−38
29	−1.9156E−53	−1.0070E−47	−3.4271E−44	−8.3839E−42	−5.1365E−40
30	+5.2087E−54	+4.6617E−49	+1.0681E−45	+1.5696E−43	−2.2156E−42
R_c	60	40	31	26	22

eccentricities ($e < 0$) through the transformation

$$N_s^- = (-1)^s N_s \tag{14}$$

where the superscript $(-)$ refers to negative eccentricities, and the N_s without a superscript refers to positive eccentricities (Table 1).

4. THE RANGE OF VALIDITY OF THE SERIES

Series such as $Nu(R) = \sum_{s=0}^{\infty} N_s R^s$ often have a limited radius of convergence, and therefore limited utility. The limited radius of convergence usually results from the presence of singularities (poles or branch points) of the function of $Nu(R)$, in the complex R plane. The singularity located closest to the origin determines the radius of convergence. The singularity may be of physical significance, indicating, for example, a bifurcation point or a limit point of some physical process; alternatively, it may lie off the real axis, and therefore have no physical significance. For examples of the above, see refs. [9, 10, 13–15].

In this section, the range of validity of the series through the use of Cauchy's root test is estimated [13, 16]

$$R_c = \lim_{s \to \infty} |N_s|^{-1/s} \tag{15}$$

where R_c is the radius of convergence. In Figs. 2(a)–(e) the variation of $|N_s|^{-1/s}$ as a function of s is depicted for the coefficients listed in Table 1. The behavior of $|N_s|^{-1/s}$ is somewhat noisy, and it is convenient to consider the even and odd terms in the series separately (open and solid circles in Fig. 2). Nevertheless, there is a clear tendency of the curves in Fig. 2 to approach an asymptotic value (dashed line in Fig. 2), which is the estimate of the radius of convergence (R_c). The radii of convergence of the series considered are listed at the bottom of Table 1. The estimates for R_c may be rough; however, a comparison of values for the Nusselt number for $R < R_c$ obtained from the series

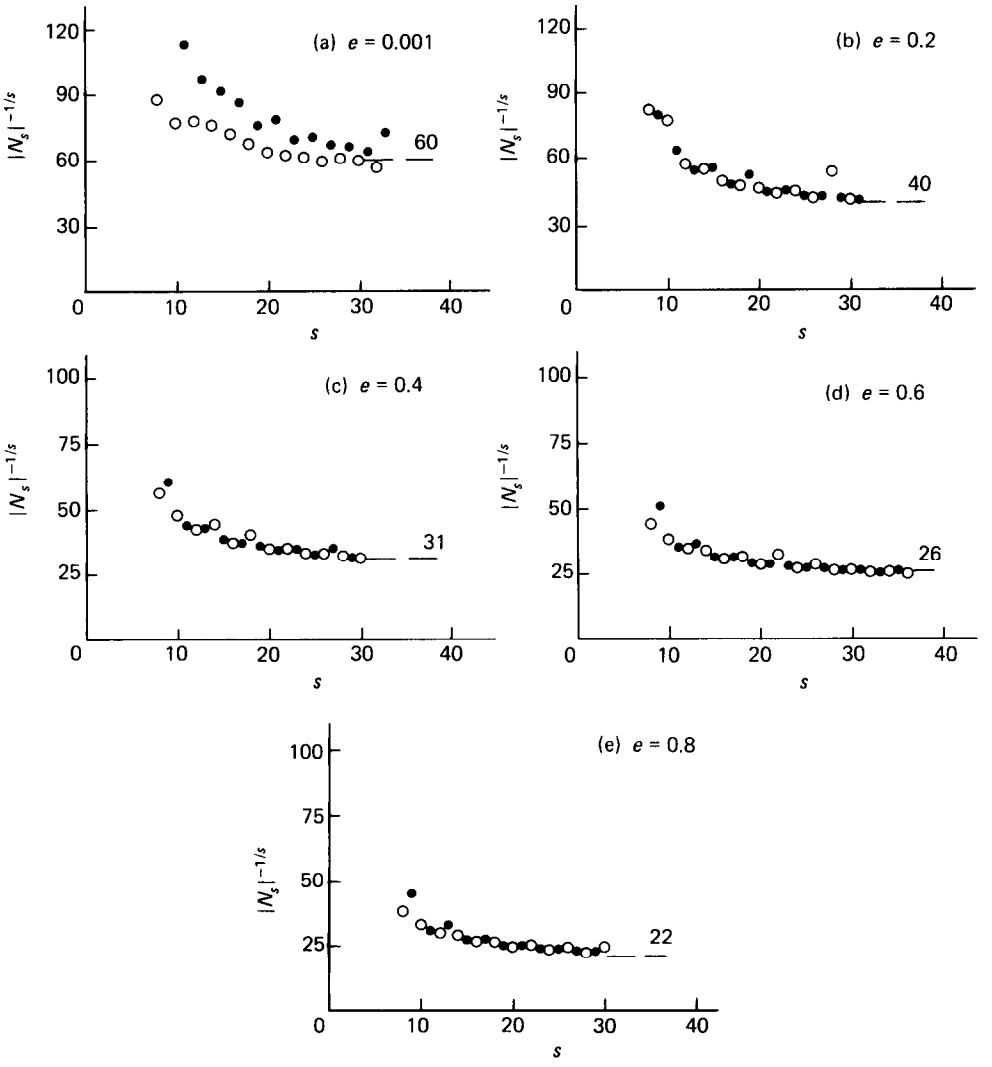

FIG. 2. Cauchy root test; the coefficients $|N_s|^{-1/s}$ are plotted as a function of s.

presentation (8) with values calculated using other techniques (Section 8) indicates that the above predictions for R_c are essentially correct. Since the Cauchy test, equation (15), is invariant to the sign of the coefficients, the same results for the radii of convergence apply for negative eccentricities as well. One can note in passing that the radius of convergence (R_c) decreases with increasing eccentricity ($|e|$).

An attempt was also made to use the ratio test [13, 16]

$$R_c = \lim_{s\to\infty} \left|\frac{N_s}{N_{s+1}}\right|. \tag{16}$$

However, the plot of $|N_s/N_{s+1}|$ as a function of s exhibits very oscillatory behavior, even when odd and even terms in series (8) are separately considered. Consequently, the ratio test does not provide any useful information in this case.

Both the erratic behavior of the coefficients (Table 1) and the oscillatory behavior of the ratio test, equation (16), suggest that the dominant singularities lie in the complex plane. An attempt was made to locate the nearest singularities by constructing new power series around various points in the region of regularity and looking for the intersection between the circles of convergence of the original and the new series. Due to an insufficient number of terms in the series, the author failed to locate the singularities within any reasonable accuracy. Nevertheless, the results do support the assertion that the nearest singularities are, indeed, complex conjugates. Additional support for this view will be provided in Section 6, where an attempt is made to locate the singularities using Padé approximants.

Thus, one can conclude that the range of validity of series (8) is limited due to non-physical singularities. In the remaining part of the paper, a variety of techniques is used in an attempt to extend the range of utility of series (8) beyond these non-physical singularities.

5. SERIES REVERSION

One can note that occasionally researchers have succeeded in extending the radius of convergence of a power series by reversing the series [9]. To see why such a procedure may work, consider, for example, the series

$$y = \ln(1+x) = x - \frac{1}{2}x^2 + \frac{1}{3}x^3 - \frac{1}{4}x^4 + \cdots$$

and the reverse series (17)

$$x = e^y - 1 = y + \frac{1}{2!}y^2 + \frac{1}{3!}y^3 + \cdots.$$

The former series converges only for $|x| < 1$ because of the logarithmic singularity at $x = -1$ while the latter has an unlimited radius of convergence.

Another example is provided in Richardson's [14] paper in which he manages to extend to infinity the radius of convergence of Blasius' series. Richardson [14] was able to achieve that by reformulating Blasius' equation and deriving the series directly from the differential equation.

Table 2. The radii of convergence of the reverted series $R = \sum_{s=1} b_s(Nu-1)^{s/2}$

	e				
	0.001	0.2	0.4	0.6	0.8
Nu_c	1.45	1.26	1.19	1.15	1.1
R_c	60	47	43	41	37

Since the coefficients (b_s) of the reverted series could not be obtained

$$R = \sum_{s=1}^{S} b_s(Nu-1)^{s/2} \tag{18}$$

from differential equations (9), one can calculate them, with some loss of accuracy, from the original series (8). For that purpose, an algorithm suggested by Van Orstand [17] is used.

The range of validity of the reveted series is estimated through the use of Cauchy's root test, in a similar fashion to what was done in the previous section. The radii of convergence for the various eccentricities are listed in Table 2. A comparison with Table 1 reveals that in this case the reversion technique is only slightly helpful. For the 'concentric' case ($e = 0.001$), there is no improvement at all, while for the eccentricity $e = 0.8$, the radius of convergence is almost doubled.

The coefficients of the reverted series (18) exhibit an erratic behavior very similar to that of the original series (8). Thus, the author proceeded by manipulating the original series (8).

6. PADÉ APPROXIMANTS

The Padé method [13, 18] consists of replacing the original series (8) with a sequence of rational functions of the form

$$\sum_{s=0}^{S} a_s R^s = \frac{\sum_{m=0}^{M} P_m R^m}{\sum_{n=0}^{N} Q_n R^n} = [M/N] \tag{19}$$

where $S = M+N+1$. Without loss of generality, $Q_0 = 1$ and the remaining $(M+N+1)$ coefficients, P_m, Q_n, are chosen so that the first $(M+N+1)$ terms in the Taylor series expansion of $[M/N]$ match the corresponding terms of the power series on the LHS of equation (19).

One considers, in particular, the 'diagonal' sequences $[M-1/M]$, $[M/M]$ and $[M+1/M]$. In Table 3, the above Padé sequences are listed for eccentricity $e = 0.6$ and Rayleigh number $R = 100$. The original power series for the Nusselt number is strongly diverging and yields the unlikely result of $Nu \sim 10^{17}$. On the other hand, all the Padé approximants in Table 3 converge rapidly to $Nu = 1.4790$, which is correct.

Through the use of the Padé approximants, one is able to significantly extend the range of utility of power

Table 3. Padé approximants, $[M-1/M]$, $[M/M]$ and $[M+1/M]$, for $e = 0.6$ and $R = 100$

M	$[M/M-1]$	$[M/M]$	$[M-1/M]$
2	1.61186013592	1.35460376571	2.5763908646
3	1.51665590489	1.48698329012	1.67696045581
4	1.53000315472	1.47345253164	1.29438826785
5	1.48498950889	1.47654498373	1.48922292522
6	1.47344589929	1.47618088254	1.47378422074
7	1.47841703234	1.47897093664	1.478708796
8	1.47832202404	1.48003202977	1.4786892798
9	1.4790488316	1.47381975707	1.479182438
10	1.47896381419	1.47918932507	1.47909305771
11	1.47898585084	1.47863611992	1.47909731172
12	1.47887893555	1.47857611962	1.47892789435
13	1.47897294747	1.47902417529	1.47906146779
14	1.47901661777	1.4790213739	1.47901254504
15	1.47901648901	1.47902450607	1.47901209087

series (8). In Table 4, for both the positive and negative eccentricities, the largest value of the Darcy–Rayleigh number (R) is listed for which all the diagonal sequences $[M+J/M]$, where $J = 0, \pm 1$, still converge within at least two significant digits. One can note that the improvement is most significant for the positive eccentricities. The application of the Padé method to the reverted series (18) yields similar results. In Table 5, estimates for the Nusselt number obtained using the Padé approximants are shown to be in good agreement with those obtained using other numerical techniques.

For the purposes of this paper, the Padé approximants are assumed to converge to the correct value if and only if all the three 'diagonal' sequences yield the same value. Thus far, a rigorous theory about the convergence of Padé approximants is available only for some special cases such as Stieltjes' series [18]. Although the present series is probably not a series of Stieltjes, there is a large body of examples available in the physics literature of situations in which the Padé approximants have yielded the correct results for series other than Stieltjes when all three 'diagonal' sequences converge to the same value [13, 18]. In view of the above and the findings in Table 5 there is strong support for the present assumption.

Next, following Gaunt and Guttmann [13], an attempt is made to locate the singularities of series (8) by examining the Padé approximants to the logarithmic derivative series (8). To this end, one surmises that $Nu(R)$ behaves like

$$Nu(R) \approx (R_c - R)^{-\eta} A(R) \quad \text{as} \quad R \to R_c^-. \tag{20}$$

Table 4. The largest value of $R = R_p$ for which all the Padé approximants converged within at least two significant digits

	e				
	0.001	0.2	0.4	0.6	0.8
			Positive eccentricities		
R_p	200	200	200	250	300
			Negative eccentricities		
R_p		100	40	40	25

Table 5. Comparison of values of the Nu number obtained from the series expansion (this paper) with numerically calculated values

R	Series solution	Padé	Galerkin	Finite difference
		$e = 0.001$		
25	1.10159	1.10159	1.100*	1.0093§
50	1.3667	1.3425	1.335*	1.335,‡ 1.3728,§ 1.328,‖ 1.363¶
100	—	1.862	1.863†	1.844,‡ 1.8286§ 1.845‖
150	—	2.26		2.26‡
200	—	(2.54)	2.66†	2.63,‡ 2.6256§
		$e = 0.2$		
25	1.09082	1.09082		
50		1.2926		1.288‡
100		1.765	1.762†	1.743‡
200		(2.59)		2.462‡
		$e = 0.4$		
25	1.0815	1.0812		—
50		1.2458		—
100		1.62		1.61‡
150		1.98		1.95‡
200		(2.3)		2.26‡
		$e = 0.6$		
25	1.0773	1.0700		—
50	—	1.1991	1.199*	—
100		1.4790	1.478†	1.465‡
150		1.744	1.77*	1.69‡
200		1.993	1.97†	1.93‡
		$e = 0.8$		
25	—	1.0530		—
50		1.1430		—
100		1.327	1.326†	1.32‡
150		1.494	1.49†	1.47‡
200		1.64	1.64†	1.62‡

* Fifteen terms were used in the Galerkin expansion.
† Sixty-six terms were used in the Galerkin expansion.
‡ Ref. [12], 1320 grid points, upwind, S.O.R.
§ Ref. [1], 1225 grid points, upwind, ADI.
‖ Ref. [2], central differences.
¶ Ref. [20], 777 grid points, upwind, S.O.R.

It follows that the logarithmic derivative

$$D(R) = \frac{\mathrm{d}}{\mathrm{d}R} \ln Nu(R) \approx \frac{\eta}{R - R_c} + \text{H.O.T. as } R \to R_c^- \tag{21}$$

has only a simple pole at R_c. Since Padé approximants can represent simple poles exactly, the poles of the approximants to the $D(R)$ series should provide a good estimate of the location of the singularities of the series $Nu(R)$. Following the above reasoning the poles and zeros of the Padé approximants to $D(R)$ were searched for. After cancelling poles with neighboring zeros one can locate for $e = 0.001$ four singularities at $\pm(18.3 \pm 0.5) \pm i(61.5 \pm 0.5)$. For larger values of the eccentricity, a larger number of singularities were found. For example, the nearest singularity for $e = 0.2$ is located at $-(26 \pm 1) \pm i(35 \pm 2)$, while the second nearest singularity is located at $-(25 \pm 1) \pm i(52 \pm 2)$. One can note that the radii of convergence corresponding to

the above singularities are slightly larger than the ones predicted by the Cauchy root test (Section 4). An attempt was also made to estimate the exponent η in equation (20) but without any conclusive results.

Thus, some support for our conjecture that the singularities which limit the range of utility of the perturbation expansion lie off the real axis is obtained. No singularities were located on the real axis.

7. SHANK'S TRANSFORMATION

An attempt was also made to use various kinds of Shank's transformations [19]. It turns out, however, that the Shank's transformations yielded similar or inferior results to those obtained through the use of Padé approximants (Section 6).

8. RESULTS AND DISCUSSION

This section consists of two parts. First, the results obtained using the series expansion (this paper) are compared with results obtained using various numerical techniques. Second, the effect of the eccentricity on the heat flow in the eccentric annulus is studied.

For the concentric annulus there is a wealth of information available in the existing literature [1–3, 20]. In Table 5 the present results for the almost concentric case ($e = 0.001$) are compared with the numerical results of others for a concentric annulus [1–3,20] and with the calculations of ref. [12]. Since there is no available data for the eccentric annulus one is forced to carry out one's own calculations, about which a few details are supplied below.

Two different numerical techniques are employed. The first one is a Galerkin procedure in which spectral expansion (12) is applied directly to the nonlinear equations (3). It was found advantageous to use only the terms on the diagonal and above. That is, the summation includes $\sum_{m=0}^{M}\sum_{n=1}^{M-m}$. By requiring that expansion (12) solves equations (3) in the sense of weighted residuals, a set of nonlinear algebraic equations is obtained for the coefficients A_{mn} and B_{mn}. The latter are solved using Newton's technique. For $R = 200$, for example, 66 spectral terms are used, which require about 10–12.5 h (a night shift) on the personal computer (HP 9816; uncompiled Basic).

The second technique is a finite-difference simulation in which the nonlinear terms are approximated using a modified-upwind scheme (Patankar's power law technique [21]). More details about the finite-difference simulation are available elsewhere [12]. One can note in passing that the finite-difference simulation exhibited instabilities for moderate Darcy–Rayleigh numbers and positive eccentricities. For example, for $e = 0.6$, $R \geqslant 300$, it was virtually impossible to obtain steady solutions. At this point, it is not clear whether these instabilities have any basis in reality or whether they are a consequence of a numerical artifact.

In Table 5 the results of the series expansion with results obtained from the numerical calculations are compared. Clearly, there is a good agreement between all these results. Thus, one has every reason to believe that the Padé approximants, indeed, converge to the correct value.

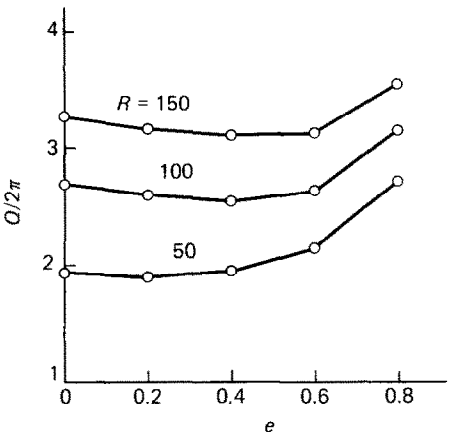

FIG. 3. The total heat flow is depicted as a function of the eccentricity for various values of the Darcy–Rayleigh number.

It is interesting to compare the series expansion with the numerical techniques from an economical point of view. The procurement of a single series expansion (30 terms) requires about 7 times the time needed to obtain a numerical solution (Galerkin technique) for a single value of the Darcy–Rayleigh number (say, $e = 0.001$, $R = 200$). On the other hand, the series expansion is valid for a whole range of Darcy–Rayleigh numbers while the numerical solution is valid only for a single Darcy–Rayleigh number. Moreover, almost the same results could have been obtained from the series expansion with a much smaller number of terms and thus with much reduced computational effort.

Finally, in Fig. 3 the variation of the total heat flow $Q/2\pi = Nu/(\alpha_1 - \alpha_2)$ as a function of the eccentricity is depicted. The results obtained from the present series expansions are denoted by circles, which are connected with straight lines in order to give a better appreciation of the trends. Clearly, as the Rayleigh number increases, there is an optimal non-zero eccentricity for which the heat transport is minimized.

A point of interest is the practical implications of this work—that is, how much energy saving can be achieved through the use of an eccentric insulator compared to the currently used concentric ones. For illustration purposes, consider a glass fiber in-

Table 6. The Darcy–Rayleigh number and estimated energy savings for a glass fiber insulation as a function of the average temperature of the insulation

T_m (K)	R	Approximate energy savings (%)
200	295	40
300	62	2.5
400	22	—

sulation saturated with air with a permeability of $\lambda = 5 \times 10^{-9}$ m^2 [22], and an equivalent thermal conductivity of 0.02 W m^{-1} K^{-1} [22], $\hat{r}_1 \div 0.5$ m, $\hat{r}_2/\hat{r}_1 = 2$, and $(\hat{T}_1 - \hat{T}_2) = 200$ K. In Table 6 the corresponding Rayleigh number for various average temperatures $(\hat{T}_m)$ of the insulation are listed. The energy savings for $R \sim 300$ were estimated from the steady-state numerical simulation. One can note that if the saturating fluid is dry air, the results are of significance only to cryogenics. The effective Rayleigh number may be much larger for cases of humid air, other saturating fluids, and/or higher permeability insulations.

9. CONCLUSION

A regular perturbation series solution has been presented for thermal convection in an eccentric annulus. The series has a limited radius of convergence due to singularities located in the complex plane. Consequently, the series is useful only for relatively small Darcy–Rayleigh numbers. The range of utility of the series can be considerably extended through the use of nonlinear transformations. Series reversion, Shank's transformation and Padé approximants were used. The latter were the most effective and enabled the Nusselt number to be calculated for up to moderate values of the Darcy–Rayleigh number ($R \sim 200$). The results obtained in this way compare favorably with results procured using numerical simulations. Finally, these results were used to demonstrate that the heat transport from an insulated pipe can be optimized by a proper choice of the eccentricity.

Nevertheless, the undertaking is only partially successful since our original objective of extending the range of utility of the series $Nu(R)$ to all Darcy–Rayleigh numbers or up to the first physical singularity (if any) has not been accomplished. Apparently, the perturbation series in this case is more difficult to analyze than other cases previously considered in the literature [9, 10]. This is due to the fact that the series $Nu(R)$ here contains a fairly large number of singularities off the real axis and to the fact that the above singularities are located fairly close to each other.

Table 7. Estimate of the accuracy of the coefficients (N_s) in the series expansion for the Nusselt number

		$e = 0.001$	
(M, N)	N_2	(M, N)	N_{11}
(15, 15)	1.72704 (−4)	(15, 15)	2.69349 (−23)
(17, 17)	1.72722 (−4)	(17, 17)	2.69346 (−23)
(18, 18)	1.72761 (−4)	(18, 18)	2.69333 (−23)
(20, 20)	1.72762 (−4)	(20, 20)	2.69334 (−23)
	N_{21}		N_{30}
(15, 15)	−1.71068 (−40)	(15, 15)	5.20244 (−54)
(17, 17)	−1.70933 (−40)	(17, 17)	5.20721 (−54)
(18, 18)	−1.70829 (−40)	(18, 18)	5.20894 (−54)
(20, 20)	−1.70783 (−40)	(20, 20)	5.20866 (−54)
		$e = 0.6$	
	N_2		N_{11}
(10, 10)	1.71225 (−4)	(10, 10)	−1.10373 (−17)
(17, 17)	1.71184 (−4)	(17, 17)	−0.91127 (−17)
(18, 18)	1.71231 (−4)	(18, 18)	−0.91157 (−17)
(20, 20)	1.71232 (−4)	(20, 20)	−0.91162 (−17)
	N_{21}		N_{30}
(10, 10)	−1.82662 (−31)	(10, 10)	−3.34306 (−43)
(17, 17)	−2.42616 (−31)	(17, 17)	1.66396 (−43)
(18, 18)	−2.42929 (−31)	(18, 18)	1.59439 (−43)
(20, 20)	−2.44279 (−31)	(20, 20)	1.56960 (−43)

Acknowledgement—This material is based upon work supported, in part, by the National Science Foundation, under grant No. MEA 8217565.

REFERENCES

1. J. P. Caltagirone, Thermoconvective instabilities in a porous medium bounded by two concentric horizontal cylinders, *J. Fluid Mech.* **76,** 337–362 (1976).
2. P. J. Burns and C. L. Tien, Natural convection in porous media bounded by concentric spheres and horizontal cylinders, *Int. J. Heat Mass Transfer* **22,** 929–939 (1979).
3. V. A. Brailovskaya, G. B. Petrazhitskii and V. I. Polezhaev, Natural convection and heat transfer in porous interlayers between horizontal coaxial cylinders, *J. Appl. Mech. Tech. Phys.* **19,** 781–785 (1978).
4. T. H. Kuehn and R. J. Goldstein, An experimental study of natural convection heat transfer in concentric and eccentric horizontal cylindrical annuli, *Trans. Am. Soc. Mech. Engrs*, Series C, *J. Heat Transfer* **100,** 635–640 (1978).
5. J. Prusa and L. S. Yao, Natural convection heat transfer between eccentric horizontal cylinders, *Trans. Am. Soc. Mech. Engrs*, Series C, *J. Heat Transfer* **105,** 108–116 (1983).
6. C. H. Cho, K. S. Chung and K. H. Park, Numerical simulation of natural convection in concentric and eccentric horizontal cylindrical annuli, *Trans. Am. Soc. Mech. Engrs*, Series C, *J. Heat Transfer* **104,** 624–630 (1982).
7. U. Projahn, H. Rieger and H. Beer, Numerical analysis of laminar natural convection between concentric and eccentric cylinders, *Num. Heat Transfer* **4,** 131–146 (1981).
8. H. H. Bau, Low Rayleigh number thermal convection in a saturated porous medium bounded by two horizontal, eccentric cylinders, *Trans. Am. Soc. Mech. Engrs*, Series C, *J. Heat Transfer* **106,** 166–175 (1984).
9. M. Van Dyke, Analysis and improvement of perturbation series, *Q. J. Mech. Appl. Math.* **27,** 423–450 (1974).
10. M. Van Dyke, Computer extension of perturbation series in fluid mechanics, *SIAM J. Appl. Math.* **28,** 720–734 (1975).
11. P. Moon and D. E. Spenser, *Field Theory Handbook.* Springer, Berlin (1971).
12. H. H. Bau, G. McBlanc and I. Saferstein, Numerical simulation of thermal convection in an eccentric annulus containing porous media, ASME 83-WA/HT-34 (1983).
13. D. S. Gaunt and A. J. Guttmann, Asymptotic analysis of coefficients, in *Phase Transition and Critical Phenomena* (edited by C. Domb and M. S. Green), pp. 181–243. Academic Press, New York (1974).
14. S. Richardson, On Blasius's equation governing flow in a boundary layer on a flat plate, *Proc. Camb. Phil. Soc.* **74,** 179–184 (1973).
15. K. L. Walker and G. M. Homsy, Convection in a porous cavity, *J. Fluid Mech.* **87,** 449–474 (1978).
16. W. Fulks, *Advanced Calculus*, pp. 379–400. Wiley, New York (1961).
17. C. E. Van Orstrand, Reversion of a power series, *Phil. Mag.* **19,** 366–376 (1910).
18. G. A. Baker and J. L. Gammel (editors), *The Padé*

Approximant in Theoretical Physics. Academic Press, New York (1970).
19. D. Shanks, Non-linear transformations of divergent and slowly convergent sequences, *J. Math. Phys.* **34**, 1–42 (1955).
20. Y. Takata, K. Fukuda, S. Hasegawa, K. Iwashige, H. Shimomura and K. Sanokawa, Three dimensional natural convection in a porous medium enclosed within concentric inclined cylinders, *ASME Conf. Proc. HTD*, Vol. 8 (1982).
21. S. V. Patankar, *Numerical Heat Transfer and Fluid Flow.* McGraw-Hill, New York (1980).
22. C. G. Bankvall, Natural convective heat transfer in permeable insulation, *Thermal Transmission Measurements of Insulation*, ASTM STP 600 (edited by R. P. Tye, pp. 73–81, American Society of Testing and Materials (1978).

APPENDIX A

In this appendix the algebraic relations resulting from the substitution of expressions (12) into equations (9) are listed.

From the momentum equation (9a) one has

$$A_{s,m,n}=\frac{-2(\alpha_1-\alpha_2)\pi^2 na}{[m^2(\alpha_1-\alpha_2)^2+n^2\pi^2]}\sum_{i=0}^{M}\sum_{j=1}^{N}B_{s-1,i,j}j[(m^2-i^2)(\alpha_1-\alpha_2)^2+(n^2-j^2)\pi^2]$$
$$\times\left\{\frac{(m+i)[\exp[-(m+i)\alpha_1]-(-1)^{j+n}\exp[-(m+i)\alpha_2]]}{[(m+i)^2(\alpha_1-\alpha_2)^2+(n-j)^2\pi^2][(m+i)^2(\alpha_1-\alpha_2)^2+(n+j)^2\pi^2]}+\frac{(m-i)[\exp[-(|m-i|)\alpha_2]-(-1)^{j+n}\exp[-(|m-i|)\alpha_1]]}{[(m-i)^2(\alpha_1-\alpha_2)^2+(n-j)^2\pi^2][(m-i)^2(\alpha_1-\alpha_2)^2+(n+j)^2\pi^2]}\right\} \tag{A1}$$

The energy equation (9b) can be written in the form

$$B_{s,m,n}=\frac{(\alpha_1-\alpha_2)}{[m^2(\alpha_1-\alpha_2)^2+n^2\pi^2]}\left[\frac{\pi}{4}\sum_{r=1}^{s=1}Q_{s,r,m,n}+mA_{s,m,n}\right] \tag{A2}$$

$$Q_{s,r,m,n}=\varepsilon_m\left\{\sum_{k=0}^{M-m}\left\{\sum_{l=1}^{n-1}A_{r,m+k,n-l}B_{s-r,k,l}(nk+ml)+\sum_{l=n+1}^{N}A_{r,m+k,l-n}B_{s-r,k,l}(-nk-ml)+\sum_{l=1}^{N-n}A_{r,m+k,l+n}B_{s-r,k,l}(ml-nk)\right\}\right.$$
$$+\sum_{k=m+1}^{M}\sum_{l=1}^{n-1}\left\{A_{r,k-m,n-l}B_{s-r,k,l}(nk-ml)+\sum_{l=n+1}^{N}A_{r,k-m,l-n}B_{s-r,k,l}(ml-nk)+\sum_{l=1}^{N-n}A_{r,k-m,l+n}B_{s-r,k,l}(-nk-ml)\right\}$$
$$+\sum_{k=0}^{m-1}\left\{\sum_{l=1}^{n-1}A_{r,m-k,n-l}B_{s-r,k,l}(ml-nk)+\sum_{l=n+1}^{N}A_{r,m-k,l-n}B_{s-r,k,l}(nk-ml)+\sum_{l=1}^{N-n}A_{r,m-k,l+n}B_{s-r,k,l}(nk+ml)\right\}\Bigg\}$$

and

$$\varepsilon_m=\begin{cases}\frac{1}{2} & \text{for } m=0\\ 1 & \text{for } m>0.\end{cases}$$

APPENDIX B

In this appendix, the accuracy of the truncated (M,N) spectral presentation (12) is examined. This is done by comparing results obtained for the coefficients (N_s) in the Nusselt number expension for various choices of (M,N). Table 7 provides a representative example. The values obtained for a few coefficients N_s are listed for the eccentricities $e=0.001$ and 0.6. For $e=0.001$ and 0.6, it is estimated that the present results are accurate within at least 4 and 3 significant digits, respectively. The deterioration in accuracy for higher eccentricities is caused by a slower convergence of the corresponding series (Appendix A). One can note that there is a deterioration in precision as the order of the terms increases.

CONVECTION THERMIQUE DANS UN ANNEAU HORIZONTAL, EXCENTRIQUE, CONTENANT UN MILIEU POREUX SATURE—UN DEVELOPPEMENT ETENDU DE PERTURBATION

Résumé—La convection thermique dans un milieu saturé poreux confiné entre deux cylindres horizontaux, isothermes, excentrés, est étudiée à partir d'un développement de perturbation en fonction du nombre de Darcy–Rayleigh (R). Les termes sont calculés jusqu'à $O(R^{30})$. En particulier, le nombre de Nusselt (Nu) est exprimé en série puissance de R pour plusieurs excentricités. Cette série puissance a néanmoins un rayon de convergence fini. Plusieurs transformations non-linéaires sont employées pour étendre le domaine d'utilisation de la série. Les résultats montrent que le transfert thermique dans l'espace annulaire peut être optimisé par un choix approprié de l'excentricité. Ces résultats ont une application à la conception des isolateurs thermiques.

THERMISCHE KONVEKTION IN EINEM HORIZONTALEN EXZENTRISCHEN RINGRAUM, DER EIN GESÄTTIGTES, PORÖSES MEDIUM ENTHÄLT—EINE ERWEITERTE STÖRUNGSRECHNUNG

Zusammenfassung—Die thermische Konvektion in einem gesättigten, porösen Medium, das zwischen zwei horizontalen isothermen exzentrischen Zylindern eingeschlossen ist, wird unter Verwendung der Darcy–Rayleigh-Zahl (R) mit Hilfe eines herkömmlichen Störungsansatzes untersucht. Dabei werden Ausdrücke bis $O(R^{30})$ berechnet. Im besonderen wird die Nusselt-Zahl (Nu) als eine Potenzreihe in R für unterschiedliche Exzentrizitäten dargestellt. Die obige Potenzreihe hat jedoch einen begrenzten Konvergenzbereich. Um den Gültigkeitsbereich der Reihenentwicklungen zu erweitern, werden verschiedene nichtlineare Transformationen herangezogen. Die Resultate zeigen, daß der Wärmeübergang in einem Ringraum durch geeignete Wahl der Exzentrizität optimiert werden kann. Diese Ergebnisse haben Einfluß auf die Gestaltung thermischer Wärmedämmungen.

ТЕПЛОВАЯ КОНВЕКЦИЯ В ГОРИЗОНТАЛЬНОМ ЗАПОЛНЕННОМ НАСЫЩЕННОЙ ПОРИСТОЙ СРЕДОЙ КОЛЬЦЕВОМ КАНАЛЕ С ЭКСЦЕНТРИСИТЕТОМ—РАЗЛОЖЕНИЕ ПО МАЛОМУ ПАРАМЕТРУ

Аннотация—Методом регулярного разложения в ряд по малому параметру с использованием числа Дарси–Рэлея (R) исследуется тепловая конвекция в насыщенной жидкостью пористой среде, которая расположена между двумя горизонтальными изотермическими цилиндрами, имеющими эксцентриситет. Расчет проводится до членов порядка R^{30}. В частности, число Нуссельта (Nu) представлено степенным рядом по R для различных значений эксцентриситета. Однако, указанный ряд имеет ограниченный радиус сходимости. Для расширения области его применимости используются различные нелинейные преобразования. На основе полученных результатов показана возможность оптимизации теплопереноса в кольцевом канале за счет соответствующего выбора эксцентриситета. Результаты исследования могут применяться при разработке теплоизоляторов.